Journal of Biomechanics 43 (2010) 1660–1666

Contents lists available at ScienceDirect

Journal of Biomechanics

journal homepage: www.elsevier.com/locate/jbiomech
www.JBiomech.com

Time and depth dependent poisson's ratio of cartilage explained by an inhomogeneous orthotropic fiber embedded biphasic model

Salman Chegini, Stephen J. Ferguson *

Institute for Surgical Technology and Biomechanics, University of Bern, Stauffacherstrasse 78, CH-3014 Bern, Switzerland

ARTICLE INFO

Article history:
Accepted 4 March 2010

Keywords:
Cartilage mechanics
Fiber embedded model
Poisson's ratio
Finite element

ABSTRACT

A time- and depth-dependent Poisson's ratio has been observed during unconfined compression experiments on articular cartilage, but existing cartilage models have not fully addressed these phenomena. The goal of this study was to develop a model which is able to predict and explain these phenomena, while also being able to fit other experimental scenarios on full depth cartilage specimens such as confined and unconfined compressions. A biphasic (poroelastic), fiber-embedded cartilage model was developed. The heterogeneous material properties of the cartilage (aggregate modulus, void ratio tensile modulus) were extracted from reported experiments on individual layers of bovine articular cartilage. The nonlinear permeability material constants were found by fitting the overall response to published experimental data from confined compression. The matrix of the cartilage was modelled as an inhomogeneous isotropic biphasic material with nonlinear strain dependent permeability. Orthotropic layers were added as embedded elements to represent collagen fibers. Material parameters for these layers were derived from tensile tests of different layers of cartilage. With these predefined tensile parameters, the model showed a good fit with multi-step confined and unconfined compression experiments (R^2=0.984 and 0.977, respectively) and could also predict the depth-dependent Poisson's ratio (R^2=0.981). The highlight of the model is the ability to explain the time-depth dependent Poisson's ratio and, by association, the strong effect of material inhomogeneity on local stress and strain patterns within the cartilage layer. This material model's response may provide valuable new insight into potential initiation of cartilage fibrillation or delamination in whole-joint simulations.

1. Introduction

Articular cartilage plays a key biomechanical role by distributing applied loads over a larger joint area, as well as providing frictionless articulation. An improved understanding of cartilage biomechanics provides pathways to better understand the pathomechanism of osteoarthritis, in which mechanical compromise and cartilage degradation are closely coupled.

Cartilage consists of a large proportion of interstitial fluid (70–90%) trapped in a porous solid media (Shapiro et al., 2001). This solid media has a very advanced structure consisting of collagen type II fibers (10–20% wet weight) and negatively charged proteoglycans (5–10% wet weight) (Mow et al., 2005), where the collagen fibers can be considered as the main frame for the containment of proteoglycans. The collagen fiber orientation varies with depth (Minns and Steven, 1977; Wilson et al., 2005) as does the concentration of fluid and proteoglycans, creating a highly heterogeneous material. The specific structure of the fibers and their constraint of being active only in tension create an inhomogeneous material with anisotropic time-dependent behaviour along with tension-compression nonlinearity (Huang et al., 2005).

To achieve a better understanding of the mechanical response of cartilage, various experimental studies have been performed. Confined and unconfined compression tests, as well as indentation tests, have been performed to characterize the compressive response (Korhonen et al., 2002). Most confined compression tests have been performed for the whole depth of the cartilage, providing the overall aggregate modulus of the cartilage, although the study by Schinagl et al., (1997) revealed a depth dependency of the aggregate modulus. Tensile tests of different layers of cartilage have been performed, concluding that cartilage has a much higher elastic modulus in tension than in compression, after relaxation, and also that the tensile modulus is highest in the superficial zone (Charlebois et al., 2004; Verteramo and Seedhom, 2004; Woo et al., 1979). Optical measurements of cartilage plugs during unconfined compression have revealed the time and depth dependent lateral displacement of cartilage (Huang et al., 2005; Jurvelin et al., 1997). Taken together, these

* Corresponding author. Tel.: +41 31 631 5925; fax: +41 31 631 5960.
E-mail address: stephen.ferguson@istb.unibe.ch (S.J. Ferguson).

0021-9290/$ - see front matter © 2010 Elsevier Ltd. All rights reserved.
doi:10.1016/j.jbiomech.2010.03.006

experiments have provided a foundation for understanding cartilage biomechanics and the basis for the development of computational models.

Cartilage models have incorporated ever more complexity to capture its behaviour in various experimental scenarios. The application of the model is an important determinant of its complexity. Cartilage has been considered as a simple incompressible linear elastic material in many whole-joint models. To account for time dependent behaviour, a viscoelastic formulation has been developed (Hayes and Mockros, 1971), followed by the biphasic/ poroelastic material models to explain the load sharing between solid and fluid phases of the tissue (Mow et al., 1980). This model was able to explain the confined compression response of the cartilage, but there was a need for further improvement to capture the response in unconfined compression. Models consisting of poroelastic media reinforced by discrete spring elements (Li et al., 2000), continuum fiber reinforced biphasic media (Garcia and Cortes, 2006; Li et al., 2009; Wilson et al., 2004), a transversely isotropic model (Bursac et al., 1999), as well as a bimodular model (Klisch, 2007) have been developed. These were able to predict the reaction force response in unconfined compression and indentation, and some were able to explain the *average* time dependent, but not depth-dependent, lateral displacement during unconfined compression (DiSilvestro and Suh, 2002). A comprehensive overview of the developed models for cartilage mechanics can be found in the review by Wilson et al., (2005), leading to the conclusion that achieving a unified cartilage model, which is able to explain the mechanical response of the cartilage in all experimental setups is a long-standing challenge.

Besides the challenge of a universal model, the pathomechanism of cartilage osteoarthritis is not completely known. The development of osteroarthritis is associated with degradation of its constituents. In studies by Lahm et al. (2009) and Saarakkala et al. (2009), the depth-wise progression of osteoarthritis in cartilage and the layer-specific degradation of collagen and proteoglycans have been explored, hinting at the need to better understand the depth-dependent properties and their influence on mechanical response.

A time- and depth-dependent lateral displacement of cartilage has been observed in various experiments (Jurvelin et al., 1997; Kiviranta et al., 2006; Wang et al., 2002) and the authors have discussed that the interaction between the cartilage constituents could be responsible for this phenomena, in that collagen fibers are activated in radial tension during unconfined compression. Although cartilage biomechanics is believed to be controlled by interaction between its constituents through the depth, there is a lack of a unified finite element model that can explain the time plus depth dependent lateral displacement of cartilage and simultaneously accurately predict the reaction force in both confined and unconfined compression. We hypothesized that a cartilage model that takes into account the heterogeneous material distribution within the depth of the cartilage, both in tension as well as compression, could enable prediction of the optically observed time and depth dependent Poisson's ratio.

2. Methods

An axisymmetric cartilage model (Fig. 1) was created, based on the experiments of Korhonen et al., (2002), in which cylindrical bovine cartilage plugs (height $h=1.15$ mm, diameter $d=3.7$ mm) were used for confined and unconfined compression tests.

The proteoglycan matrix and the interstitial fluid (without collagen fibers) was represented as a biphasic material with a depth-dependent aggregate modulus extracted from the experimental data of Schinagl et al., (1997), where the total height of the cartilage was divided into 9 equal layers. The aggregate modulus of individual layers was reported as (0.079, 0.10, 0.17, 0.27 and 0.55 MPa) descending from the superficial zone, more uniform in layers six through eight (0.58–0.73 MPa) and increasing steeply in the ninth layer (1.14 MPa), close to the calcified cartilage interface. Following the experiments of Jurvelin et al., (1997), where an incompressible behaviour was observed during fast loading, along with the incompressibility of the fluid, the Poisson ratio of the proteoglycan matrix was set to 0.499. This biphasic media was assumed to be fully saturated, in which a depth-dependent fluid volume fraction (Shapiro et al., 2001) was defined as follows:

$$V = 0.9 - 0.2(z/h) \tag{1}$$

where z is the depth from articulating surface and h is the total specimen height.

A nonlinear strain dependent permeability was used for the layers described in the following equation (Lai et al., 1981)

$$k = k_0 e^{(M\varepsilon)} \tag{2}$$

where k_0 is the initial permeability at zero strain, and M is a dimensionless material parameter.

To account for the tensile properties of the cartilage, reinforcing layers were added to the biphasic isotropic proteoglycan matrix using the "embedded element" option in ABAQUS 6.6 (Dassault Systemes Simulia GmbH, Aachen, Germany). This constrains the nodal displacements of the embedded media (here the media representing the fiber contribution) to the biphasic continuum (representing the proteoglycan matrix and interstitial fluid). The material properties of these orthotropic layers were extracted from published tensile experiments on thin cartilage specimens (Charlebois et al., 2004; Verteramo and Seedhom, 2004; Woo et al., 1979), and formulated so that their overall behaviour matched the tensile experiments of different layers of cartilage in the radial direction. An exponential curve was fit to the experimental tensile data of superficial zone cartilage (Charlebois et al., 2004) :

$$\sigma_{\exp} = A(\exp(B\varepsilon) - 1)(\text{MPa}) \tag{3}$$

where $\sigma_{\exp}$ is the tensile stress in the cross section of the cartilage layer and ε is the tensile strain. A and B were calculated as 6.1 and 1.05, respectively.

Reducing the contribution of the proteoglycan matrix from the stress function, the stress within the reinforcing layers is defined as follows:

Stress in the radial and axial direction (respectively):

$$\sigma_L^r = \{\sigma_{\exp} - \sigma_m(\text{if } \varepsilon^r > 0), \quad \sigma_L{}^r \approx 0(\text{if } \varepsilon^r < 0)\} \tag{4}$$

$$(z):\ \sigma_L^z \approx 0$$

where σ_L^r is the radial tensile stress in the reinforcing layer and σ_m signifies the tensile stress in the biphasic media. σ_L^z is the compressive stress in axial direction for the reinforcing layers.

The tensile stress-strain function for the middle zone and deep zone was set to 50% and 38%, respectively, of the superficial layer (Verteramo and Seedhom, 2004).

The orthotropic tensile properties of the layers were applied through a user material subroutine (UMAT) in the model. The axisymmetric geometry was meshed using a 450 CAX4P (4 nodes, linear, axisymmetric with fluid pressure degrees of freedom) elements for the biphasic media and the embedded orthotropic layers were meshed with 450 CAX4 elements with material properties defined within the subroutine.

Displacement was applied to the model following the experiments of Korhonen et al., (2002), during which stepwise stress–relaxation tests (each step 5% of uncompressed cartilage thickness, velocity 1 μm/s) were applied up to a maximum 20% strain, followed by relaxation in each step, for both confined and unconfined compression.

To simulate confined compression, a free draining boundary condition was applied to the upper surface, the radial displacements of the symmetry line and right edge were constrained, and all the displacement degrees of the bottom layer were fixed to zero. By fitting the model response to the experimental measurements using an unconstrained nonlinear minimization routine (Matlab, MathWorks Inc., 2004), the permeability material constants (k_o, M) were calculated for confined compression.

The reaction force during the unconfined compression was compared with experimental measurements for validation. The boundary conditions were such that draining was allowed only at the right edge of the model, at the lateral side of the cartilage plug. The radial displacement of the symmetry line and axial displacement of the bottom layer were fixed and the stepwise displacement was applied to the upper layer of the cartilage followed by relaxation as mentioned above. The predicted change in the lateral displacement of the cartilage model was recorded as a function of time and depth, and compared with another set of independent experiments (Wang et al., 2002; Jurvelin et al., 1997) to verify the main hypothesis of the study. A flowchart of model development and validation is shown in Fig. 2.

A control case model was created for comparison using an average aggregate modulus of 0.4 MPa (Schinagl et al., 1997) and tensile material constants of $A=2.5$ MPa and $B=1.0$ (in Eq. 3), to compare the apparent Poisson's ratio and stresses with those calculated by the depth-dependent model.

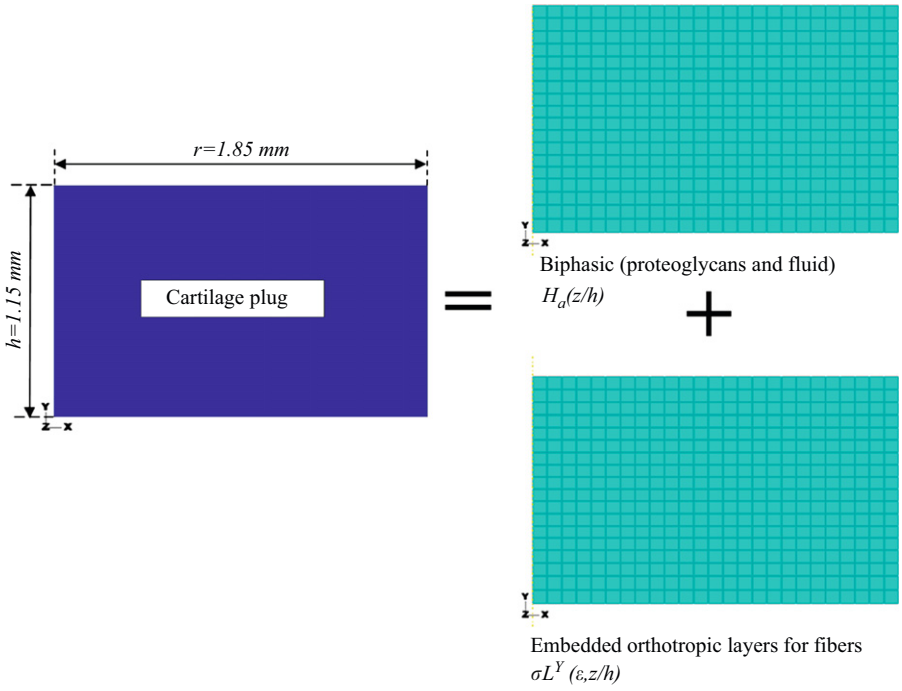

Fig. 1. Geometry of the cartilage plug (left) and the mesh of the biphasic layers (upper right) as well as embedded orthotropic layers (lower right).

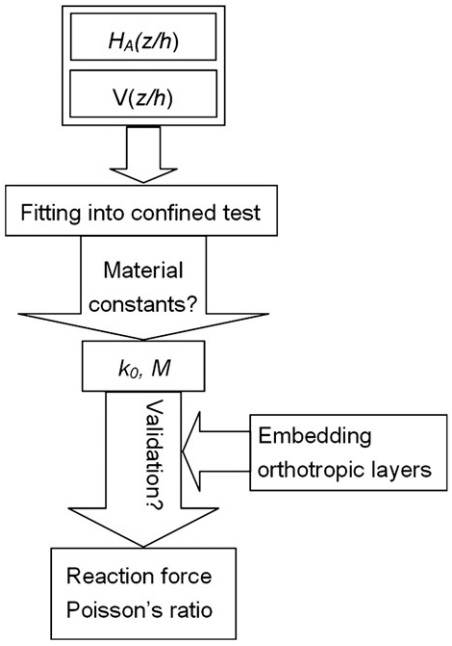

Fig. 2. Schematic work flow for finding the material parameters and validation of the model.

3. Results

By fitting the overall response of the model in confined compression to experimental data, the material parameters were calculated as $k_0^s = 5 \times 10^{-15}$ m^4/N.s and $M = 2.3$, respectively. The correlation coefficient between the model results and experimental data was $R^2 = 0.984$ (Fig. 3). The results of the simulation for the four steps of unconfined compression are compared with experimental data in Fig. 4 and show a good correlation coefficient of $R^2 = 0.977$. The model can predict the reaction force at low strains (up to 15% axial strain) but fails to

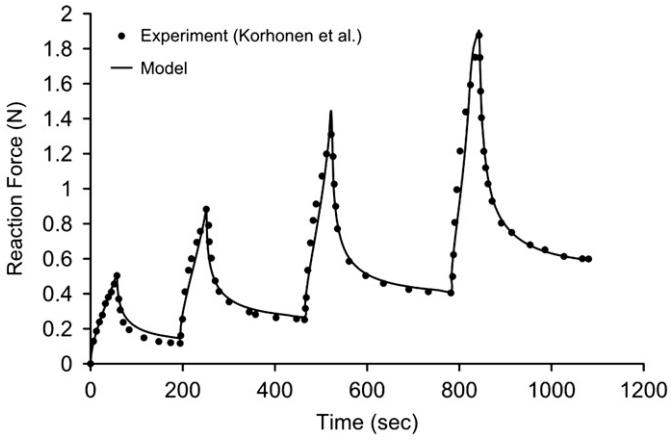

Fig. 3. Comparison of the model response after fitting to confined compression experiments (Korhonen et al., 2002).

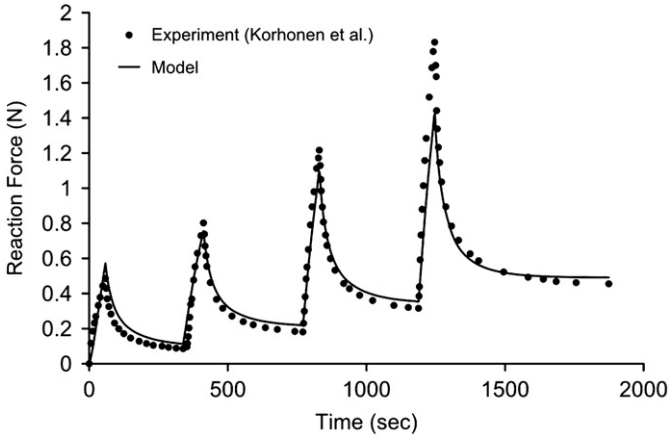

Fig. 4. Comparison of the model response with the unconfined compression experiments (Korhonen et al., 2002).

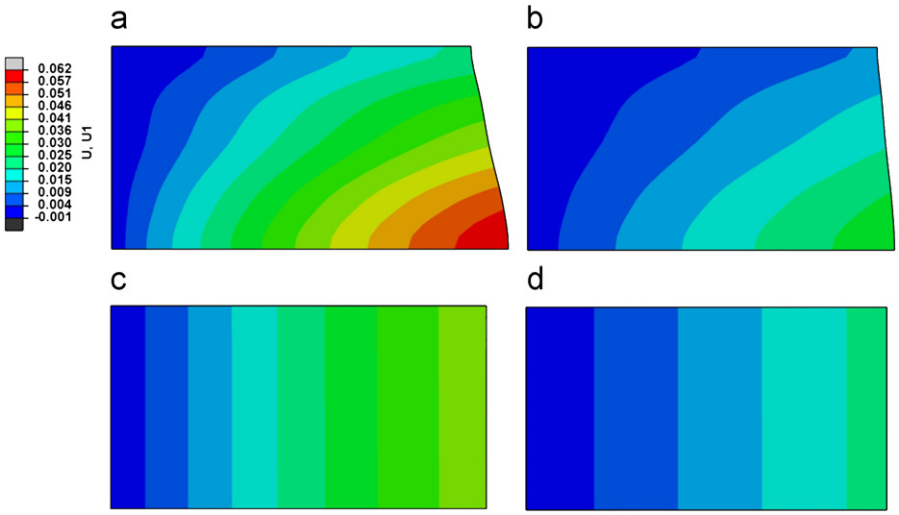

Fig. 5. Lateral displacement of the cartilage (5 times magnified) (a) the fiber reinforced model after 10% nominal strain of unconfined compression, (b) fiber reinforced model after relaxation, (c) control model after 10% strain, (d) control model after relaxation.

fully capture the high reaction force in the 20% axial strain scenario. Relative errors in reaction force for 5%, 10%, 15% and 20% strains were 2%, 11%, 20% and 28%, respectively.

The lateral displacement of the cartilage under unconfined compression loading is shown in Fig. 5 (magnified 5 times in the radial direction) before and after the relaxation, to show the effect of the fluid drainage on the lateral displacement. After application of the platen displacement, the cartilage expanded laterally (Fig. 5a), but this expansion reduced as the interstitial fluid drained out (Fig. 5b). The superficial layer tends to expand less than the deeper layers. On the other hand, the lateral displacement for the control case remains constant throughout the depth but reduces as a function of time (Fig. 5c,d).

The Poisson's ratio of the cartilage, as a function of normalized depth after relaxation, is plotted in Fig. 6a. The Poisson's ratio is compared with the experiments reported by Wang et al., (2002) for both the depth-dependent and control models. The results of the depth-dependent model followed the experiment and stayed within the overall variation of experiments, however with a maximum error of 27%, which occurred in the deepest zone.

The time dependency of the Poisson's ratio in different zones during relaxation is plotted in Fig. 6b, which shows the reduction of the Poisson's ratio as the fluid drains. In fact, Fig. 6a presents the relaxed Poisson's ratio, which is provided for three discrete zones in Fig. 6b, and the corresponding endpoints are marked. The model prediction for time-dependent Poisson's ratio are compared with experimental results of Jurvelin et al. (1997) for the deep zone (Fig. 6c), where an instantaneous displacement of 5% nominal axial strain was applied in the experimental study, followed by relaxation, and the presented model describes 50 s of loading followed by relaxation. The maximum error between the model and experiments was 15%, at the end of loading step.

In addition to the external values of lateral displacement, the internal strains and stresses within the biphasic matrix and the embedded orthotropic fiber layers of the cartilage are plotted for both the depth dependent and control model (Fig. 7a–f) for the relaxed state after application of 10% axial strain.

4. Discussion

Introducing more detailed experimental data through depth dependent tensile and aggregate moduli to the cartilage model enables a single model to capture time- and depth-dependent zonal behaviour as well as predicting the overall response of the cartilage in both confined and unconfined compression. Of note, the tensile material properties were predefined in this model, not obtained through a best fit of the model response.

The predicted Poisson's ratio from the depth-dependent model is in relatively good agreement with the optically measured Poisson's ratio during unconfined compression (Jurvelin et al., 1997; Wang et al., 2002), where it follows the trend of average Poisson's ratio and lies within the variation from several independent experiments with different bovine cartilage samples. A closer fit could be obtained through optimizing model response by allowing variation of the individual tensile modulus values; however our goal was to test a modelling philosophy in which tensile modulus values were predetermined by reported values.

The Poisson's ratio is lowest in the superficial zone, which has the highest tensile modulus. This supports the view of Kiviranta et al., (2006), who discussed that the Poisson's ratio is primarily controlled by collagen fibers, but since only an average bulk modulus was incorporated in the analysis of Kiviranta et al., there was no report on depth dependency of Poisson's ratio. This could be due to not considering modulus variation through the depth. Previous finite element fiber-reinforced models also assumed a constant aggregate modulus for the whole matrix, and therefore are able to predict time dependent average lateral displacement (Wilson et al., 2004), but not the depth dependency. The present study supports that the collagen network controls the tensile modulus throughout the cartilage depth, and this in turn determines the depth-dependent Poisson's ratio. If an average aggregate modulus and tensile modulus is used, the Poisson's ratio is constant through the depth (Fig. 6a). Although there have been experimental and theoretical studies on the subject, this is the first finite element study to address this phenomenon.

The theoretical model of Wang et al. (2003) has shown that the relaxed Poisson's ratio may vary from 0.06–0.38, depending on the aggregate modulus, which is in accordance with their experiments (0.04–0.28). Also, a recent study by Ateshian et al., (2009) showed that implementing the matrix and fiber constituents and taking the tension-compression nonlinearity into account enables the model to predict many observed phenomena. The presented study is in line with the findings of Ateshian et al.,

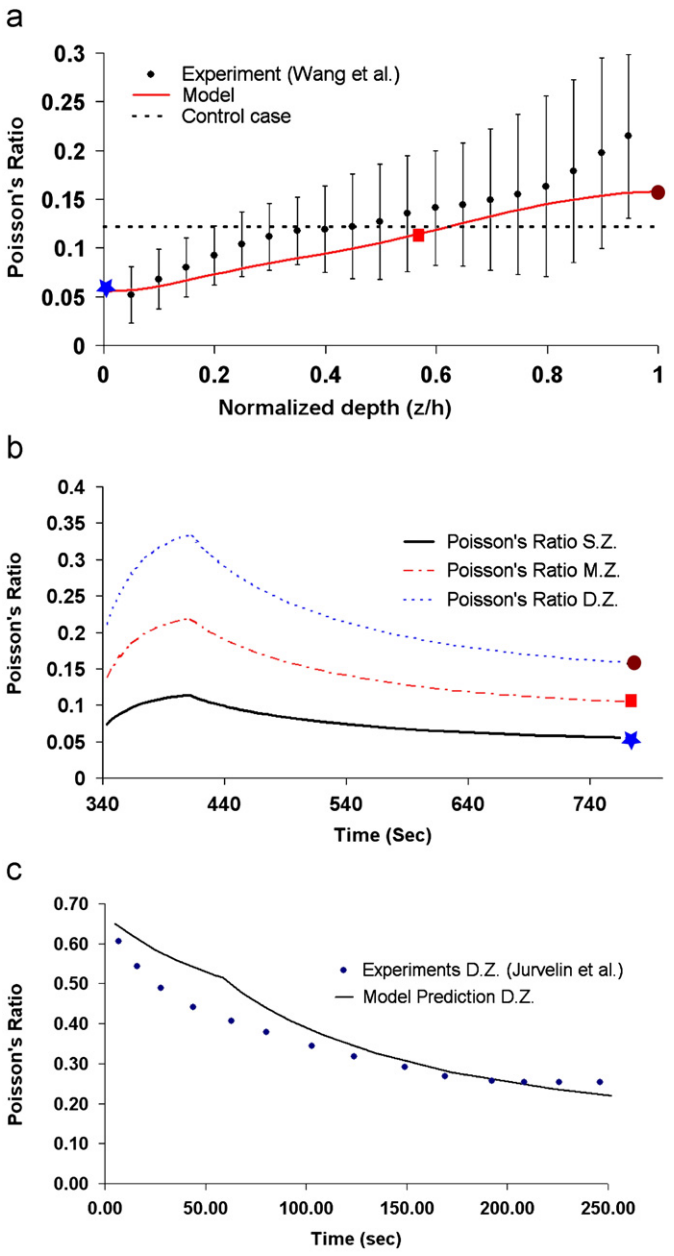

Fig. 6. (a) Depth dependent Poisson's ratio after 10 % axial strain followed by relaxation (b) time dependent Poisson's ratio for superficial zone (SZ), middle zone (MZ) and deep zone (DZ) during loading and relaxation, (c) comparison of relaxation of Poisson's ratio of deep zone with experimental results of Jurvelin et al. (1997).

using a different methodology, and furthermore captures the time dependency of lateral displacement for different zones. Nevertheless, a detailed analysis of the relative contribution of the tension-compression non-linearity and the heterogeneous distribution of properties would be a valuable topic of future study.

The observed instantaneous incompressible behaviour of cartilage (Jurvelin et al., 1997) can be explained by incompressibility of the interstitial fluid and the proteoglycan matrix, which together comprise most of the cartilage volume fraction. During unconfined compression, tensile strains are induced in the radial direction; the collagen fibers embedded in the matrix exert forces to counteract lateral expansion. As fluid drains from the lateral surfaces, driven by the contracting fibers, the total volume is reduced and therefore the effective Poisson's ratio of the composite tissue, analogous to the optically observed ratio, is less than the intrinsic Poisson's ratio defined for the matrix.

The resulting radial strains in the biphasic matrix for the depth-dependent model (Fig. 7a) and control model (Fig. 7b) differ, such that the highest radial strain is observed in the deepest zone for the depth-dependent model. This is due to the lower tensile fiber modulus in the deep zone, which allows a preferential radial expansion of the matrix. Whereas the internal matrix stresses and fiber layer stresses in the control model are homogeneous (Fig. 7d and f, respectively), the stresses in the depth dependent model are strongly heterogeneous (Fig. 7c and e). This is relevant for the prediction of tissue failure. Local areas of high deformation could be considered initiation points for tissue fibrillation or delamination and these local peaks are not predicted by a homogeneous model. Incorporation of the heterogeneous distribution of tissue properties in a full-joint model could identify local maxima of distortion, under simulated physiological loading, and provide a better understanding of the potential mechanism of cartilage failure under semi-confined loading.

Recently, the development of non-invasive diagnostic approaches for determining the degree of osteoarthritis have been proposed, by measuring the reaction force during in situ indentation, (Kiviranta et al., 2008; Brown et al., 2007) and/or deriving local Poisson's ratio (Julkunen et al., 2008). One future use of the present model could be a more detailed prediction and comparison of the depth-dependent Poisson's ratio of osteoarthritic cartilage with healthy cartilage. To this end, the properties of osteoarthritic cartilage, including the depth-dependent aggregate and tensile modulus, would be required. The results of the study show a strong dependency of the local stress and strain state on the heterogeneous spatial distribution of the constituents (Fig. 7). Further extension of the study, by implementing the spatial distribution of constituents in degraded cartilage from (Lahm et al., 2009) and Saarakkala et al., (2009), could explain how the stress distribution progresses in various stages of degeneration.

There are parameters, which have not been taken into account in the present study. The viscoelasticity of the fibers (layers) is not considered in this study. If a step tensile load is applied to cartilage, its relaxation rate is so high that most of the relaxation occurs within about 20 s after load application (Huang et al., 2001). In this study, the model has been compared with test scenarios where there was no instantaneous loading; therefore the viscous properties of the fibers were not taken into account. Adding the viscosity of the layers may further strengthen the model to fit data from fast loading scenarios. The hyper-elasticity of the aggregate modulus has been observed during confined compression experiments (Chen et al., 2001), but since the strain dependency was reported not to be considerably large, it was neglected in this study. This may be the reason why the model could not predict the high reaction force during unconfined compression for higher strains (Fig. 4). It should be noted that a model without fibers was not able to capture the reaction force response during unconfined compression, which is one of the main inspirations for development of most fiber-reinforced models. Therefore, it is plausible that the reaction force during unconfined compression is influenced by interaction between the biphasic matrix and the fibers, which are in tension, thus not including the complex behaviour of each part would result in deviation from the actual reaction force. Inclusion of depth-dependent initial permeability may also improve the prediction of reaction forces (Huang et al., 2005; Chen et al., 2001; Wilson et al., 2007). An isotropic permeability was used for this study, although some studies have shown that the permeability is direction dependent (Reynaud et al., 2006). While we speculate

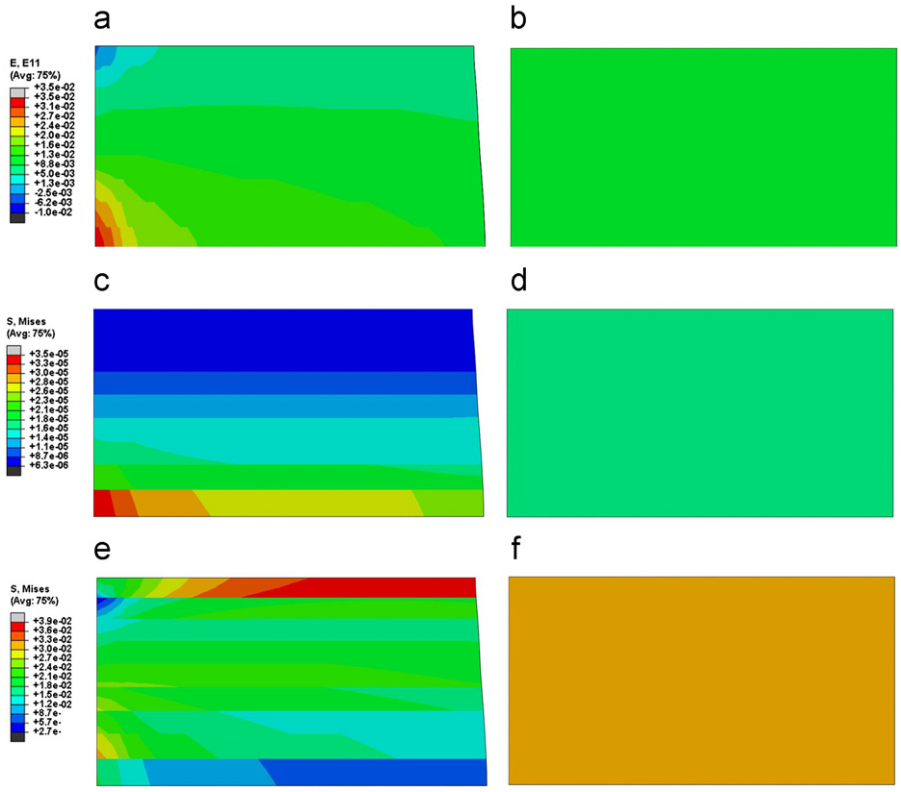

Fig. 7. Comparison of the radial tensile strains in the biphasic matrix in the case of the depth dependent model (a) and the control case (b) after 10% applied strain and relaxation. Comparison of the von Mises equivalent stresses (MPa) in the biphasic matrix in case of the depth dependent model (c) and the control case (d) and in the embedded orthotropic fiber layers in case of the depth dependent model (e) and the control case (f) at the same time. The model with depth-dependent properties predicts a highly heterogeneous local stress and strain response.

that the short-term response (effective incompressibility of constituents) and long-term response (fully drained state) would not be strongly influenced by the degree of direction dependency, anisotropic permeability will alter the relative rate of lateral contraction and internal rearrangement for the transient (relaxation) response. This should be addressed in future studies.

In conclusion, the depth dependent tensile and aggregate properties of cartilage control the depth dependent Poisson's ratio and are therefore important for the accurate prediction of reaction forces and internal stress distribution during unconfined compression. Time dependency of the Poisson's ratio is the result of interaction between the tensioned fibers, that tend to restore the original shape of the cartilage, and the biphasic matrix that needs time for draining of interstitial fluid. More detailed experimental measurements of tensile modulus for thinner layers of the cartilage would enable the model to predict the Poisson's ratio more accurately.

Conflict of interest statement

Authors have no financial or personal relationships that could inappropriately influence or bias this work.

Acknowledgement

Funding was provided by the Swiss National Science Foundation (NCCR CO-ME).

References

Ateshian, GA, Rajan, V, Chahine, NO, Canal, CE, Hung, CT., 2009. Modeling the matrix of articular cartilage using a continuous fiber angular distribution predicts many observed phenomena. J. Biomech. Eng. 131 (6), 061003.

Brown, C.P., Crawford, R.W., Oloyede, A., 2007. Indentation stiffness does not discriminate between normal and degraded articular cartilage. Clin. Biomech. 22, 843–848.

Bursac, P.M., Obitz, T.W., Eisenberg, S.R., Stamenovic, D., 1999. Confined and unconfined stress relaxation of cartilage: appropriateness of a transversely isotropic analysis. J. Biomech. 32, 1125–1130.

Charlebois, M., McKee, M.D., Buschmann, M.D., 2004. Nonlinear tensile properties of bovine articular cartilage and their variation with age and depth. J. Biomech. Eng. 126, 129–137.

Chen, A.C., Bae, W.C., Schinagl, R.M., Sah, R.L., 2001. Depth- and strain-dependent mechanical and electromechanical properties of full-thickness bovine articular cartilage in confined compression. J. Biomech. 34, 1–12.

DiSilvestro, M.R., Suh, J.K., 2002. Biphasic poroviscoelastic characteristics of proteoglycan-depleted articular cartilage: simulation of degeneration. Ann. Biomed. Eng. 30, 792–800.

Garcia, J.J., Cortes, D.H., 2006. A nonlinear biphasic viscohyperelastic model for articular cartilage. J. Biomech. 39, 2991–2998.

Hayes, W.C., Mockros, L.F., 1971. Viscoelastic properties of human articular cartilage. J. Appl. Phys. 31, 562–568.

Huang, C.Y., Mow, V.C., Ateshian, G.A., 2001. The role of flow-independent viscoelasticity in the biphasic tensile and compressive responses of articular cartilage. J. Biomech. Eng. 123, 410–417.

Huang, C.Y., Stankiewicz, A., Ateshian, G.A., Mow, V.C., 2005. Anisotropy, inhomogeneity, and tension-compression nonlinearity of human glenohumeral cartilage in finite deformation. J. Biomech. 38, 799–809.

Julkunen, P., Korhonen, R.K., Herzog, W., Jurvelin, J.S., 2008. Uncertainties in indentation testing of articular cartilage: a fibril-reinforced poroviscoelastic study. Med. Eng. Phys. 30, 506–515.

Jurvelin, J.S., Buschmann, M.D., Hunziker, E.B., 1997. Optical and mechanical determination of Poisson's ratio of adult bovine humeral articular cartilage. J. Biomech. 30, 235–241.

Kiviranta, P., Rieppo, J., Korhonen, R.K., Julkunen, P., Toyras, J., Jurvelin, J.S., 2006. Collagen network primarily controls Poisson's ratio of bovine articular cartilage in compression. J. Orthop Res. 24, 690–699.

Kiviranta, P., Lammentausta, E., Töyräs, J., Kiviranta, I., Jurvelin, J.S., 2008. Indentation diagnostics of cartilage degeneration. Osteoarthritis Cartilage 16, 796–804.

Klisch, S.M., 2007. A bimodular polyconvex anisotropic strain energy function for articular cartilage. J. Biomech. Eng. 129, 250–258.

Korhonen, R.K., Laasanen, M.S., Toyras, J., Rieppo, J., Hirvonen, J., Helminen, H.J., Jurvelin, J.S., 2002. Comparison of the equilibrium response of articular cartilage in unconfined compression, confined compression and indentation. J. Biomech. 35, 903–909.

Lahm,A., Mrosek,E., Spank,H., Erggelet,C., Kasch,R., Esser,J., and Merk,H. (2010) Changes in content and synthesis of collagen types and proteoglycans in osteoarthritis of the knee joint and comparison of quantitative analysis with Photoshop-based image analysis. Arch. Orthop. Trauma Surg. 130 (4), 557–564.

Lai, W.M., Mow, V.C., Roth, V., 1981. Effects of nonlinear strain-dependent permeability and rate of compression on the stress behavior of articular cartilage. J. Biomech. Eng. 103, 61–66.

Li, L.P., Buschmann, M.D., Shirazi-Adl, A., 2000. A fibril reinforced nonhomogeneous poroelastic model for articular cartilage: inhomogeneous response in unconfined compression. J. Biomech. 33, 1533–1541.

Li, L.P., Cheung, J.T., Herzog, W., 2009. Three-dimensional fibril-reinforced finite element model of articular cartilage. Med. Biol. Eng. Comput. 47, 607–615.

Minns, R.J., Steven, F.S., 1977. The collagen fibril organization in human articular cartilage. J. Anat. 123, 437–457.

Mow, V.C., Chen, A.C., Wong, Y.G., 2005. Structure and function of articular cartilage and meniscus. In Basic Orthopaedic Biomechanics pp. 181–258, Philadelphia.

Mow, V.C., Kuei, S.C., Lai, W.M., Armstrong, C.G., 1980. Biphasic creep and stress relaxation of articular cartilage in compression? theory and experiments. J. Biomech. Eng. 102, 73–84.

Reynaud, B, Quinn, TM, 2006. Anisotropic hydraulic permeability in compressed articular cartilage. J. Biomech. 39 (1), 131–137.

Saarakkala,S., Julkunen,P., Kiviranta,P., Makitalo,J., Jurvelin,J.S., and Korhonen,R.K. (2010) Depth-wise progression of osteoarthritis in human articular cartilage: investigation of composition, structure and biomechanics. Osteoarthritis. Cartilage 18 (1), 73–81.

Schinagl, R.M., Gurskis, D., Chen, A.C., Sah, R.L., 1997. Depth-dependent confined compression modulus of full-thickness bovine articular cartilage. J. Orthop. Res. 15, 499–506.

Shapiro, E.M., Borthakur, A., Kaufman, J.H., Leigh, J.S., Reddy, R., 2001. Water distribution patterns inside bovine articular cartilage as visualized by 1H magnetic resonance imaging. Osteoarthritis.Cartilage 9, 533–538.

Verteramo, A., Seedhom, B.B., 2004. Zonal and directional variations in tensile properties of bovine articular cartilage with special reference to strain rate variation. Biorheology 41, 203–213.

Wang, CC, Chahine, NO, Hung, CT, Ateshian, GA., 2003. Optical determination of anisotropic material properties of bovine articular cartilage in compression. J. Biomech. 36 (3), 339–353.

Wang, C.C., Deng, J.M., Ateshian, G.A., Hung, C.T., 2002. An automated approach for direct measurement of two-dimensional strain distributions within articular cartilage under unconfined compression. J. Biomech. Eng. 124, 557–567.

Wilson, W., Huyghe, J.M., van Donkelaar, C.C., 2007. Depth-dependent compressive equilibrium properties of articular cartilage explained by its composition. Biomech. Model. Mechanobiol. 6, 43–53.

Wilson, W., van Donkelaar, C.C., van Rietbergen, B., Ito, K., Huiskes, R., 2004. Stresses in the local collagen network of articular cartilage: a poroviscoelastic fibril-reinforced finite element study. J. Biomech. 37, 357–366.

Wilson, W., van Donkelaar, C.C., van Rietbergen, R., Huiskes, R., 2005. The role of computational models in the search for the mechanical behavior and damage mechanisms of articular cartilage. Med. Eng. Phys. 27, 810–826.

Woo, S.L., Lubock, P., Gomez, M.A., Jemmott, G.F., Kuei, S.C., Akeson, W.H., 1979. Large deformation nonhomogeneous and directional properties of articular cartilage in uniaxial tension. J. Biomech. 12, 437–446.